data

MDPI

Data Descriptor

Digital Elevation Models and Orthomosaics of the Dutch Noordwest Natuurkern Foredune Restoration Project

Gerben Ruessink [1,*], Dick Groenendijk [2] and Bas Arens [3]

[1] Department of Physical Geography, Faculty of Geosciences, Utrecht University, 3584 CS Utrecht, The Netherlands
[2] PWN Drinking Water Company, 1991 AS Velserbroek, The Netherlands; dick.groenendijk@pwn.nl
[3] Bureau for Beach and Dune Research, 3768 CA Soest, The Netherlands; arens@duinonderzoek.nl
* Correspondence: b.g.ruessink@uu.nl

Abstract: Coastal dunes worldwide are increasingly under pressure from the adverse effects of human activities. Therefore, more and more restoration measures are being taken to create conditions that help disturbed coastal dune ecosystems regenerate or recover naturally. However, many projects lack the (open-access) monitoring observations needed to signal whether further actions are needed, and hence lack the opportunity to "learn by doing". This submission presents an open-access data set of 37 high-resolution digital elevation models and 24 orthomosaics collected before and after the excavation of five artificial foredune trough blowouts ("notches") in winter 2012/2013 in the Dutch Zuid-Kennemerland National Park, one of the largest coastal dune restoration projects in northwest Europe. These high-resolution data provide a valuable resource for improving understanding of the biogeomorphic processes that determine the evolution of restored dune systems as well as developing guidelines to better design future restoration efforts with foredune notching.

Dataset: https://doi.org/10.5281/zenodo.7010095

Keywords: foredune; coastal dunes; restoration; UAV; photogrammetry; airborne laser scanning; wind; digital elevation model; orthomosaic; monitoring

Citation: Ruessink, G.; Groenendijk, D.; Arens, B. Digital Elevation Models and Orthomosaics of the Dutch Noordwest Natuurkern Foredune Restoration Project. *Data* **2024**, *9*, 37. https://doi.org/10.3390/data9020037

Academic Editor: Juanle Wang

Received: 31 January 2024
Revised: 8 February 2024
Accepted: 10 February 2024
Published: 15 February 2024

1. Summary

Coastal dunes are intrinsically valuable ecosystems along most of the world's sandy beaches, whose dynamics are determined by plant–geomorphic feedback [1–3]. They also contribute directly or indirectly to human well-being by protecting against coastal hazards and providing drinking water and space for recreation [4,5]. Human activities related to, for example, urban expansion and development for tourism, increasingly damage, degrade, or destroy dune habitats around the world [6–9]. To reverse this trend of negative transformation, restoration measures are being taken in more and more dune areas to create conditions that allow the dunes to naturally return to a previous biogeomorphic trajectory [10–15]. The number of ways in which dunes can be restored is enormous [9,16,17] and includes efforts to replant sand patches to restore or build dunes [15,18–20] as well as efforts to remove vegetation to reactivate aeolian dynamics and locally reset ecological succession [10,12,14]. The way in which restored dunes will develop is often highly uncertain due to the long time scales involved (years to decades), the legacy of pre-restoration conditions (e.g., any remaining seeds or rhizomes) [21], the non-linearity of biogeomorphic feedback, and changing boundary conditions (e.g., due to global change). Therefore, many restoration projects are adaptively managed based on evidence [22,23]. Monitoring is essential not only to see if the imposed measures are working and if additional actions are needed, but also to "learn by doing". However, since (non-)governmental organisations or consultants

are often responsible for monitoring, the resulting data usually remain part of the "grey literature" [16,24] and are not easily accessible to improve scientific understanding of the biogeomorphic feedback underlying the changes of restored dunes and to help practitioners develop guidelines to better design future efforts.

The aim of this data descriptor paper is to make available a unique open access data set (CC BY 4.0) of remotely sensed digital elevation models (DEMs) and orthomosaics from the Noordwest Natuurkern (NWNKern) project in Zuid-Kennemerland National Park, located along the west coast of the Netherlands (Figure 1a). The NWNKern project, one of the largest coastal dune restoration projects in northwest Europe, involved the excavation of five artificial trough blowouts (also termed "notches" [12,14]) through the foredune in winter 2012/2013 (Figure 1). The project aimed to reactivate aeolian sand dynamics and geomorphological diversity in order to increase the area of the Natura 2000 habitat type H2120 Shifting dunes along the shoreline with European marram grass (*Calamagrostis arenaria*, formerly *Ammophila arenaria*) or "White dunes" and, second, improve conditions for habitat type H2130 Fixed coastal dunes with herbaceous vegetation or "Grey dunes" [25]. The latter is expected, at least in part, from the inland suspension of fine calcareous material; its deposition as grainfall up to hundreds of metres landward of the foredune [26] can limit soil acidification [27]. Although the project was started to expand and restore coastal dune habitats, it was soon realised that the inland transport of windblown sand through the notches would also benefit long-term coastal safety by facilitating elevation gain of the inland dunes and therefore their vertical growth with sea level rise [21]. The data set includes 35 DEMs and 24 orthomosaics collected between 2013 and 2023, and two pre-excavation DEMs from 2008 and 2012. An analysis of geomorphological changes during the first years after notch excavation can be found in [12] and of the data set up to October 2021 in [28]. Preliminary work on the classification of habitats from orthomosaics can be found in [29–31].

2. Data Set Description

2.1. Study Site

The five NWNKern notches, labelled N1 to N5 from south to north, are located in an approximately 1 km stretch of the 20 m high established foredune between Bloemendaal aan Zee in the south and IJmuiden in the north (Figure 1a). In recent decades, the beach sediment budget has been moderately positive [32,33], mainly due to the impact of the 2.5 km long IJmuiden harbour moles on waves and currents near the coast and probably also related to various sand nourishments on the beach of Zandvoort aan Zee, 6 km to the south. The foredune borders a low-gradient intertidal beach and an upper beach with incipient foredunes up to 2.5 m high (embryo dunes) on its sea side and an ≈5 km wide dune system with vegetated parabolic dunes and dune slacks on its land side. Vegetation was removed from several parabolic dunes as part of the NWNKern project [25,34] (e.g., P1–P3 in Figure 1b,c). Most of the national park is part of the European Natura 2000 network of protected nature areas. The most common habitat types in the vicinity of the notches are the aforementioned White (H2120) and Grey (H2130) dunes, together with "dunes with sea buckthorn *Hippophae rhamnoides*" (H2160, often together with wild privet *Ligustrum vulgare*) and "humid dune slacks" (H2190) [35]. The sediment consists of medium sand, with the median grain size fining from 300 to 350 µm on the beach to 250–300 µm in the notches.

A total of 170,000 m^3 of sand was excavated in winter 2012/2013 to create the five notches. As detailed in [12], the notches had a V shape (viewing landward) through the foredune, with the notch floor starting at approximately 6 m above Mean Sea Level (MSL) at the seaward side and sloping linearly to about 9 m +MSL at the landward side. N2 and N1 were the narrowest (50 m) and widest (100 m) notches, respectively, while the cross-dune length of the notch floor was the smallest for N1, N2, and N3 (100 m) and largest for N5 (200 m). The maximum excavation depth ranged between 9 m for N3 to 12.5 m for N5. The three southern notches (N1–N3) are approximately normal to the coast, while the two northern notches (N4 and N5) have a more southwest–northeast orientation

(Figure 1b). The notches deliberately had different characteristics (width, depth, orientation, perimeter) in order to investigate which combination of characteristics would result in the largest landward aeolian sand transport.

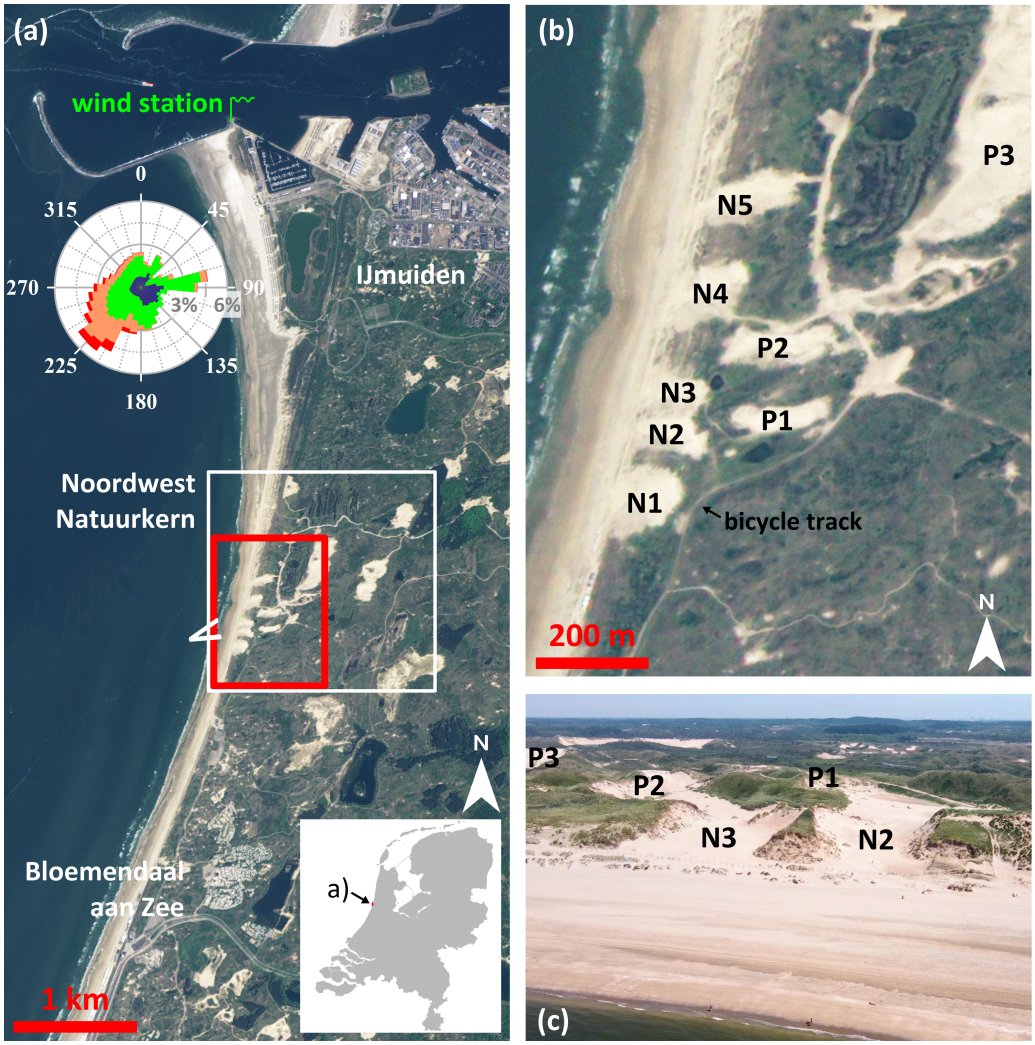

Figure 1. (**a**) Location of the study site along the west coast of the Netherlands. The white rectangle indicates the approximate region in which the foredune and landward dunes were reactivated as part of the Noordwest Natuurkern project, visible as the bare sand areas landward of the beach. The area containing the five foredune notches, which is the focus of this paper, is outlined by the red rectangle and is shown in more detail in (**b**). The five notches are labelled N1 to N5 from south to north. Three reactivated parabolic dunes (P1–P3) are also indicated. (**c**) Photo of part of the notched foredune, looking east–northeast. Panels (**a**,**b**) contain the pansharpened Formosat-2 RGB satellite image (2 m resolution) of 27 May 2013, shortly after the excavation of the notches was completed. The photo in (**c**) was taken with a drone in summer 2021. The white open triangle in (**a**) is the approximate view angle of the photo in (**c**). The wind rose in (**a**) contains four wind speed classes: dark blue, $\leq$5 m/s; green, >5–10 m/s; orange, >10–15 m/s; red, >15 m/s.

The Netherlands experiences a temperate oceanic climate. The annual mean wind speed in the North Sea in front of the Dutch coast is about 8 m/s. In winter, the mean wind speed is substantially higher ($\approx$9.5 m/s) than in summer ($\approx$6.5 m/s). The highest 10-min average wind speed varies from year to year but is typically in the range of 21 to 25 m/s. The predominant direction of the wind is from the southwest (Figure 1a). Storms, especially those from the northwest, can raise the tidal water level by 1 m or more (storm surge), but dune erosion at the site is rare due to the wide intertidal beach and the wave sheltering by

the IJmuiden harbour moles during these conditions. Annual rainfall amounts to about 800 mm.

The site experienced a variety of human activities after notch excavation. Some of these measures were planned in advance given the experience in nearby restoration measures [21,36], and other activities happened to be in the study area but were not related to the NWNKern restoration measures. In 2013 and 2014, marram grass was manually removed from the mouth of the notches. Several times, the rubble from the notch floors was mechanically removed (sieving). The rubble is primarily made up of small concrete blocks or bricks that come from bunkers on the Atlantic wall from World War II or from an abandoned bicycle track and beach entrance. Part of the sand blown on the current bicycle track landward of the southernmost notch (N1; Figure 1b) was bulldozed to the beach (≈900–1500 m^3 per year between 2013 and 2016) or elsewhere on the depositional lobe (e.g., in December 2020), but this practice was subsequently abandoned and the track has since been buried under several metres of sand. The N1 notch is a public beach entrance ("Strandslag Kattendel"), but the other notches are closed to the public. Beachgoers could walk freely between the incipient foredunes on the upper beach, but this region was fenced off in spring 2023 to create roosting and breeding places for coastal birds (project "Groene Strand"). A club for catamaran sailors and surfers was located at the base of the foredune south of N1 until summer 2017. Finally, in summer 2019, a section of incipient dunes north of the northernmost notch (N5) was cleared to detonate several World War II bombs found near Schiphol airport. The absence of these dunes caused a significant (windblown) supply of sand on and beyond the foredune in subsequent autumn–winter periods. The deposits were so thick in places that marram grass and small sea buckthorn shrubs were completely buried. In subsequent years, vegetation has recolonised most of the foredune, but the embryo dunes had not fully recovered by the end of 2023.

2.2. Morphological Data

The core of the data set consists of 37 digital elevation models (DEMs) and 24 orthomosaics collected between 10 May 2008 and 25 September 2023. The survey dates are provided in the Open Document Spreadsheet file `NWNKern_Surveys_ErrorStatistics.ods`, Sheet `NWNK`, Column `B` as YYYY-MM-DD, where YYYY, MM, and DD are the year, month, and day of the survey, respectively. The first two DEMs (2008-05-10 and 2012-02-20) show the situation before the notch excavation, the third DEM (2013-01-14) during the excavation, and the other 34 DEMs, starting from 2013-05-01, show the morphological evolution after the excavation work was completed. DEMs were computed from survey data collected with different remote sensing techniques (`NWNKern_Surveys_ErrorStatistics.ods`, column `C`): airborne laser scanning (ALS, 14 surveys), lidar from an uncrewed aerial vehicle (UAVLidar, 2 surveys), and UAV-acquired Structure-from-Motion photogrammetry (UAVSfM, 21 surveys). Orthomosaics are available for all 23 UAV surveys and a single ALS survey, as indicated with `Y` in `NWNKern_Surveys_ErrorStatistics.ods`, column `E`; otherwise, an `N` is provided in this column.

The DEMs are provided as GeoTIFF files named `NWNKern_YYYYMMDD_METHOD_Zf.tif`, where `NWNKern` is the abbreviation for the research site, `METHOD` is ALS, UAVLidar, or UAVSfM, and `Zf` indicates that the file contains gap-filled (f, see Section 3) elevation Z. The horizontal coordinate system is Amersfoort/RD New (EPSG:28992). The horizontal axes are easting (X) and northing (Y) and are orientated east and north, respectively. The unit of measure is metres, m. Elevation is in m with respect to Normaal Amsterdams Peil (NAP), with a positive value above NAP. The value $Z = 0$ m NAP corresponds approximately to the mean sea level. The DEMs have a rectangular grid with a resolution of 1 m. The lower left corner coordinates (X_{ll},Y_{ll}) are (98,300, 492,900) m, and the upper right corner coordinates (X_{ur},Y_{ur}) are (99,200, 494,100) m. Each grid thus measures 900 × 1200 m; its outline is shown in Figure 1a with the red box and corresponds precisely to Figure 1b. The 900 × 1200 Z values in each DEM are provided for the centres of the grid cells. The NoData

value for Z is −9999. Additional cartographic information and grid properties can be read from the metadata in the GeoTIFF files.

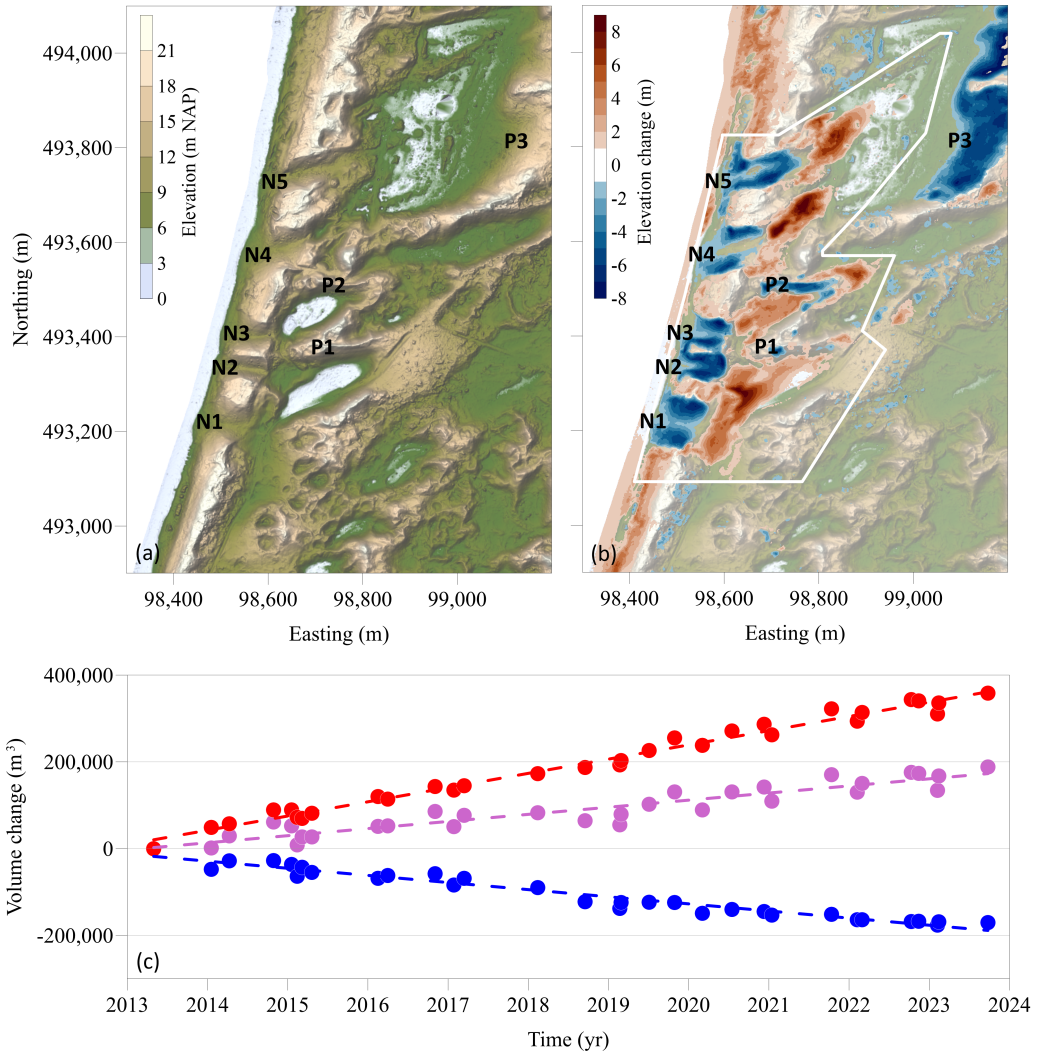

Figure 2. (**a**) Digital elevation model of the 2013-05-01 survey, shown as a colour relief map and (**b**) DEM of Difference for 2013-05-01–2023-02-08. Positive elevation change represents deposition. The background is the colour relief map of (**a**) with an opacity of 60%. Elevation change ±1 m is completely transparent. (**c**) Time series of deposition volume V_d (red dots), erosion volume V_e (blue dots), and net volume change V_n (magenta dots) for the region bounded by the polygon (white line) in (**b**), relative to the 2013-05-01 survey. The dashed lines are the best-fit linear lines. Their statistics are given in the text. The tick marks on the horizontal axis in (**c**) are, as in all subsequent figures with a time axis, at the start of the year.

The 2013-05-01 DEM is provided as an example in Figure 2a and clearly illustrates the five excavated notches. The morphological change in the available data set is demonstrated with the DEM of Difference (DoD) for 2013-05-01–2023-02-08 in Figure 2b, with positive, and negative difference values corresponding to deposition and erosion, respectively. The DoD shows that depositional lobes have formed landward of the notches, locally almost 10 m thick and extending to 300 m inland. Sand was also deposited on the foredune remnants between the notches (rim deposition) and on the seaward side of the foredune to the south and north of the five notches. Erosion is concentrated in the five notches, especially at the lateral walls (locally up to almost 9 m), and at the reactivated parabolic dunes, most notably P2 and P3. Time series of deposition volume V_d, erosion volume V_e, and net volume change V_n (Figure 2c) were calculated for a polygon (Figure 2b) with its

seaward side on the upper beach to exclude changes in beach volume from the calculations and its landward side to capture the evolution of the notches and lobes throughout the interval of available DEMs. The polygon is provided in the repository with the GeoJSON file `notches.geojson`. Volumes are taken relative to the 2013-05-01 DEM, and therefore the time series show the cumulative morphological evolution after the excavation of the notches. At the end of the time series in September 2023, V_d and V_e were approximately 360,000 and −170,000 m^3, respectively, implying a net sand gain since May 2013 of about 190,000 m^3 (Figure 2c). The three time series show an approximately linear trend over time, with best fit slopes m of 32,785 ± 1552, −16,405 ± 1354, and 16,380 ± 2283 m^3/yr (±values are the 95% confidence interval) and correlation coefficients r of 0.99, −0.98, and 0.94 for V_d, V_e, and V_n, respectively.

Orthomosaics are available as 8-bit GeoTIFF files with three bands (band 1: red; band 2: green; band 3: blue) and are named `NWNKern_YYYMMDD_RES.tif`. Here, `RES` is 005 or 100 for 0.05 or 1.00 m square grid resolution. The corner coordinates in all orthomosaic files are identical to those in the DEM files. With the 1 m resolution the orthomosaic grids are thus identical to those of the DEMs. The 0.05 m resolution files have 18,000 × 24,000 pixels and are provided for improved visualisation purposes as well as for future studies on vegetation dynamics. NoData in the orthomosaics is expressed by the colour white. Examples of orthomosaics are provided in Figure 3.

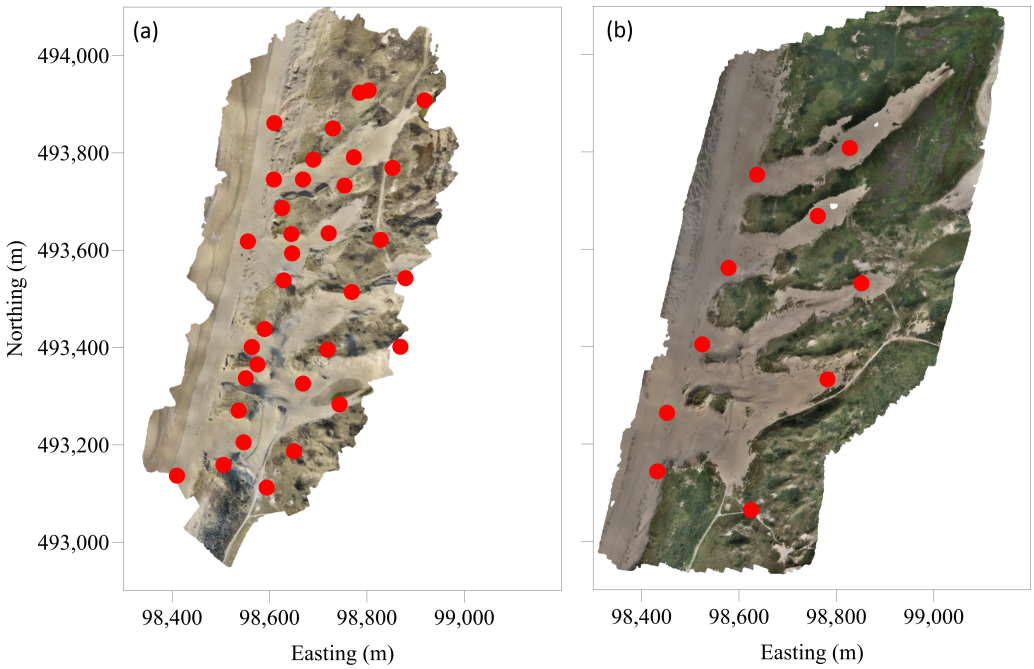

Figure 3. Orthomosaics of the (**a**) 2017-03-15 and (**b**) 2023-09-25 surveys. The red dots are the locations of the ground control point (GCP) targets used in the Structure-from-Motion workflow, described in Section 3.1. Panels (**a**) and (**b**) contain 37 and 10 GCPs, respectively.

2.3. Meteorological Data

To advance future studies on the biogeomorphic evolution of the study region, the morphological data set is supplemented with high-frequency times series of wind characteristics and rainfall. Both series span the time period between 1 January 2008 and 31 December 2023 with a resolution of 10 minutes and were obtained from the Royal Netherlands Meteorological Institute Data Platform (https://dataplatform.knmi.nl/, accessed most recently on 8 January 2024).

Wind observations (Figure 4a) from the weather station (IJmuiden WMO 06225, see Figure 1a; 52°27.733 N, 004°33.300 E) are available in the data repository with the ASCII space-delimited file `windIJmuiden.txt`. The file has seven columns: year, month, day, hour,

minute, wind speed, and wind direction. The time is in UTC +01:00 (Mean European Time), the wind speed is in m/s, and the direction in °N. Both wind variables are at a height of 10 m, and NoData values are indicated with NaN. Also shown in Figure 4a are the 24 storm events in the period 2013–2023. Notable are the four storms in January–February 2022 (named Corrie, Dudley, Eunice, and Franklin), the last three of which occurred within a week (16–20 February). The highest 10-min average wind speed (31.4 m/s) was measured during the storm on 5 July 2023, named Poly. The wind rose of the observations is provided in Figure 1a.

Rainfall observations (Figure 4b) are provided for the Wijk aan Zee weather station (WMO 06257; 52°30.316 N, 004°36.182 E, which is in the dunes northeast of the northern IJmuiden harbour mole), with the ASCII space-delimited file `rainfallWijkAanZee.txt`. The file has six columns: year, month, day, hour, minute, and rainfall intensity in millimetres per hour. As in the wind file, the time is in UTC +01:00 and the NoData value is NaN. The median annual rainfall in the period 2008–2023 was about 810 mm; the highest annual rainfall was recorded in 2023 (1113 mm).

The IJmuiden and Wijk aan Zee stations were chosen for two reasons: they are the two stations closest to the study site where wind and rain are measured by the Royal Netherlands Meteorological Institute, respectively, and they are located near the foredune. Therefore, they can be considered the most representative stations for the study region.

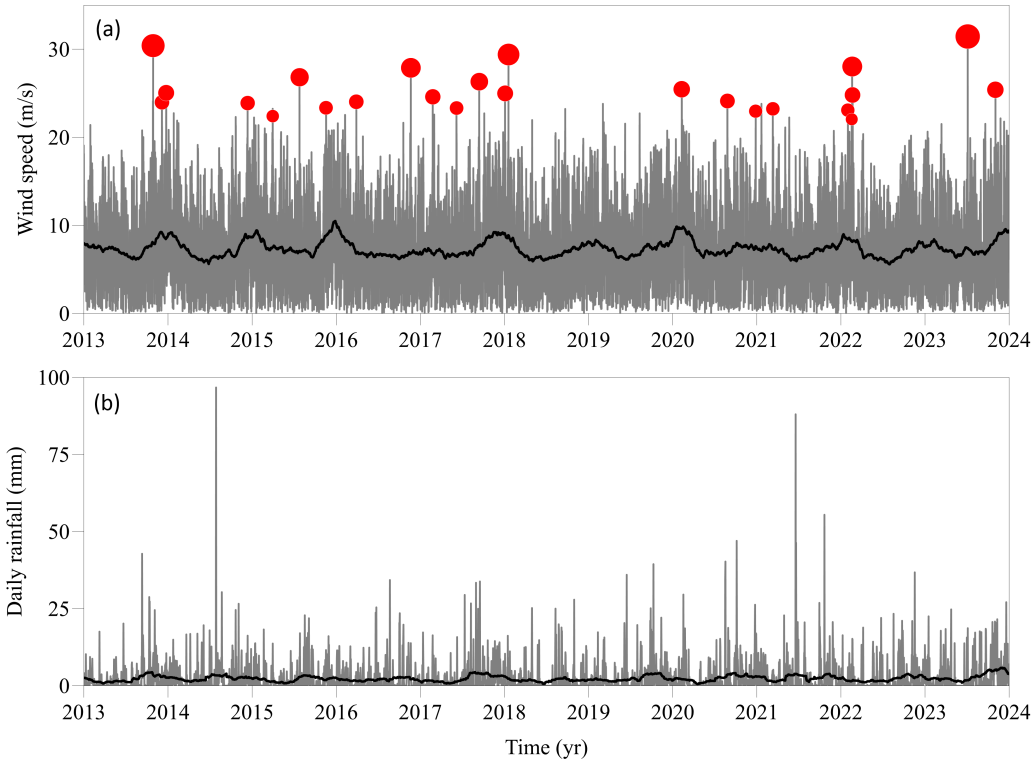

Figure 4. Time series of meteorological data for the NWNKern region 2013–2023: (**a**) wind speed at IJmuiden WMO 06225; grey lines are 10-min average values, dark line is 90-day moving average, and red dots are storm events for which at least 6 consecutive 10-min wind speeds exceed 20.7 m/s (i.e., event duration is at least 1 h). The dots are plotted at the peak of the storm and scale with peak wind speed. (**b**) Rainfall at Wijk aan Zee WMO 06257; grey lines are daily amounts, and dark line is 90-day moving average. The shown time period is the same as in Figure 2c.

3. Methods

3.1. Uncrewed Aerial Vehicle Structure-from-Motion (UAVSfM) Photogrammetry

UAV surveys to acquire true-colour aerial images (RGB) suitable for SfM processing have been conducted on average 2 to 3 times per year since 1 May 2013. The first image data set was collected with a fixed-wing Trimble X100 by a commercial contractor (Kragten,

Herten, The Netherlands). All subsequent surveys were conducted by drone experts from Utrecht University, first with a fixed-wing Easystar–I equipped with a 12.1 Mpix Canon Powershot D10 and from July 2019 with a DJI Phantom 4 RTK quadcopter with a 20 Mpix camera. The Phantom 4 has centimeter-level accuracy Real-Time Kinematic (RTK) positioning on-board; spatially interpolated RTK-correction data were provided during surveying by a commercial service provider, 06-GPS.nl. The coordinate scheme for the Phantom 4 camera locations was ETRS89 (EPSG:4258). Before SfM processing, the coordinates were converted to Amersfoort/RD New (EPSG:28992) and NAP elevation with Trimble® Business Center software, v. 2.81.4686.41842. The images collected with the Trimble X100 and Easystar–I did not have location information. Two surveys (2020-03-09 and 2021-04-26) had to be abandoned prematurely for logistical reasons and contained part of N1 only. The 2018-04-19 survey was considered completed in the field, but it turned out to be missing part of N1 during processing. These three surveys are indicated with `N` in `NWNKern_Surveys_ErrorStatistics.ods`, column `D` ('uncompleted'); otherwise, `Y` is provided in this column ('completed'). The latter does not imply that the entire grid has elevation values; instead, it implies that the DEM contains all the notches and depositional lobes.

Ground control point (GCP) targets were deployed during each survey to be used in the SfM workflow and to georeference the images. Although Phantom 4 images were directly georeferenced, we found, consistent with previous studies [37,38], that a small number of GCPs considerably improved the accuracy of image locations, especially elevation. Up to 40 GCPs were placed throughout the study region, with a smaller number (typically 10) during Phantom 4 surveys (compare Figure 3a with 3b). The actual number of placed GCPs is provided in `NWNKern_Surveys_ErrorStatistics.ods`, column `G`. The GCPs had circular or checked black-and-white patterns. Their centres were measured with a Trimble® RTK-GPS receiver, connected to 06-GPS.nl, with a horizontal and vertical accuracy of approximately 0.02 and 0.04 m, respectively. The GCP coordinate scheme was Amersfoort/RD New with elevation with respect to NAP.

SfM processing was performed in Agisoft Metashape Pro (v. 1.8.4), except for the May 2013 survey, for which we do not have details of the workflow. The workflow for all other UAV image data sets was based on the guidelines in [39] and consisted of the following main steps, all performed with an Ubuntu 2.04 Virtual Machine with a single A10 GPU in the HPC SURF Research Cloud:

1. All images were imported into a new Agisoft project, as were camera locations and orientations with their associated error estimates, if available. Image quality was calculated, and poor quality images, often due to motion blur, were disabled. When applicable, the sea surface was masked in the images. The images were aligned in the high-quality setting, with a keypoint limit of 40,000 and unlimited tiepoints.
2. Low-quality tiepoints were selected and removed in several consecutive steps. First, obvious outliers were manually selected and removed. Second, tiepoints were selected and removed based on reconstruction uncertainty, projection accuracy, and reprojection error, for which threshold values of 10, 3, and 0.3 were applied, respectively. After each selection and removal step, the internal and external camera parameters were optimised. The thresholds mentioned are target values. Depending on how many tiepoints would actually be removed, the threshold values were sometimes relaxed [39].
3. The GCPs were imported into the project and subsequently used (1) to georeference the point cloud (or, in Phantom 4 surveys, to improve the georeferencing based on camera locations and orientations) and (2) to optimise the internal camera parameters. Columns `H-K` in `NWNKern_Surveys_ErrorStatistics.ods` provide statistics of the XYZ residuals of the GCPs as the X, Y, Z and 3D ('total') root mean square (rms) errors. The maximum 3D rms error for complete surveys was 0.05 m (2015-04-21). For most Phantom 4 surveys, the total rms error was less than 0.02 m. The error statistics for the first five EasyStar–I surveys (2014-04-10–2016-04-01) provided here are lower

than in [12] due to improvements in the selection and removal of low-quality tiepoints (step 2).

4. A dense point cloud was calculated using medium-quality and aggressive filtering settings. Points with a confidence of less than 3 were removed, as well as off-terrain points due to cars, wooden posts, information signs, garbage bins, animals, or people. No attempt was made to remove off-terrain points due to vegetation; this is discussed in Section 4. Then, a polygonal mesh model was calculated, which was finally used to generate an orthomosaic with ground-pixel resolution (<0.05 m) using the mosaic blend mode (default).

The orthomosaics provided in the repository were exported from the Agisoft project with 0.05 and 1.0 m resolution. Each dense point cloud was exported in LAZ format and subsequently processed into a DEM using MATLAB® [40] (R2023a; https://nl.mathworks.com/, accessed most recently on 30 January 2024). The LAZ file was read into MATLAB® using the `lasFileReader` function of the Lidar toolbox. Elevation Z at each location was taken as the average Z of all points within a search radius equal to the grid resolution (here, 1 m). These points were found using a $k-d$ tree search method, implemented in the `rangesearch` function of the Statistics and Machine Learning toolbox. Regions without Z data that were entirely surrounded by grid points with data were subsequently filled with Laplace interpolation, implemented in the TopoToolbox (v. 2) [41].

3.2. Lidar from An Uncrewed Aerial Vehicle (UAVLidar)

The company Shore Monitoring & Research performed lidar surveys on 17 September 2018 and 22 February 2019 using a DJI Matrice 600 Pro UAV equipped with an AL3-32 mobile laser scanner from Phoenix LiDAR Systems. For each survey, the collected point cloud was filtered to retain only ground points and provided as a LAZ file, with horizontal coordinates in Amersfoort/RD New (EPSG:28992) and elevation with respect to NAP. The LAZ file was processed into a DEM as described in the UAVSfM workflow (Section 3.1). The UAV was also equipped with an RGB camera. The aerial images collected were processed by Shore Monitoring & Research with Agisoft PhotoScan Professional to an orthomosaic with a resolution of 0.02 and 0.10 m. These orthomosaics were resampled at a resolution of 0.05 and 1.0 m using the gdal software package (https://gdal.org/, accessed most recently on 30 January 2024) for inclusion in the data set presented in this paper.

3.3. Airborne Laser Scanning (ALS)

All ALS point clouds except 2015-02-13 were collected as part of the annual Coastal Lidar campaign of the Dutch government organisation Rijkswaterstaat [42–44] and are publicly available in LAZ format from https://downloads.rijkswaterstaatdata.nl/, accessed most recently on 30 January 2024. The 2015-02-13 survey was commissioned by PWN, the nature manager of the study region, and the acquired data were provided as ASC Arc/Info ASCII grids with 0.5 m resolution. For the purpose of the present work, these files were merged and converted to LAZ format. The PWN-commissioned survey also resulted in an orthomosaic of the NWNKern region. ALS surveys were generally conducted in January, February, or March, prior to the start of the growing season. The point clouds were corrected for vegetation and additional off-terrain objects by the commercial contractors who performed the data collection. The horizontal coordinates are in the Amersfoort/RD New system (EPSG:28992) and the elevation is with respect to NAP. Data quality documents illustrate that elevation data meet the requirements of Rijkswaterstaat, having a bias less than 0.05 m and a standard deviation less than 0.1 m. Because the focus of the annual campaign until 2022 was on the beach and the foredune, the most landward part of the depositional lobes was missing from the point clouds. Inquiries with Rijkswaterstaat revealed that Lidar data points have been collected landward of the foredune since 2016 but have not been processed as standard into the publicly available point clouds. For the present data set, these additional points were made available and merged with the point clouds of the beach and the foredune. Rijkswaterstaat indicated that the quality of these

additional data may deviate from the requirements. The 2008 and 2014 ALS point clouds do contain high-quality data points landward of the foredune, because these surveys were carried out simultaneously with the second and third national-scale AHN campaigns (https://www.pdok.nl/introductie/-/article/actueel-hoogtebestand-nederland-ahn, accessed most recently on 30 January 2024). From 2023, Rijkswaterstaat expanded the area for lidar data collection and processing in the NWNKern region far landward of the depositional lobes. Each ALS point cloud was processed into a DEM in the same way as described for the UAVSfM point clouds.

4. User Notes

The DEMs in the present data set are based on two remote sensing techniques: laser scanning (UAVLidar and ALS) and Structure-from-Motion photogrammetry (UAVSfM). Laser pulses can, at least partially, penetrate through the canopy, and the resulting point cloud comprises vegetation and ground points. With a suitable filter method, vegetation points can be selected and removed (as was performed here), implying that the resulting DEM is a Digital Terrain Model (DTM), also in vegetated areas. If the vegetation is very dense, ground points cannot be found; this might be the case on the marram-grass-covered foredune. Structure-from-Motion does not result in ground points beneath the canopy, and hence a DEM based on UAVSfM is a Digital Surface Model (DSM), including the elevation of the canopy [45–47]. The difference between a DTM and a DSM is illustrated in Figure 5a, which shows the DoD between the ALS DEM of 2023-02-08 and the UAVSfM DEM of 2023-02-13. Because the two surveys were conducted only five days apart (with mainly low wind conditions), we can safely assume that the calculated elevation change actually represents the height of the canopy. The DoD shows a clear cross-shore zonation. A canopy height of up to 0.6 m is mostly found on the seaward side of the foredune south and north of the notches, on the foredune between the notches, and along the edges of some depositional lobes. At these locations, the vegetation is dominated by marram grass (habitat H2120, White dunes) [29]. Further inland, canopy heights to over 2 m can be seen, most notably on the seaward side of the foredune south of N1 and north of N5. These higher canopy elevations correspond to dark green vegetation patches in the orthomosaic of 2023-09-25 (that is, taken in the growing season of the same year, when the vegetation is more clearly visible; Figure 5b). These dark green patches are sea buckthorn and wild privet shrubs (habitat H2160) [29]. Figure 5 also shows that substantial parts of vegetated inland dunes are not associated with notable differences between the two DEMs, for example, to the east and south of the depositional lobes of N1 and N2. Here, the dominant habitat is H2130 (Grey dunes) with centimetre-high lichens and mosses and other short plants [29].

The presence of DTMs (UAVLidar and ALS) and DSMs (UAVSfM) in the data set raises the question to what extent the volume computations in Figure 2c were affected by vegetation-induced bias in the DSMs. Therefore, an analysis of covariance (ANOCOVA) was performed to evaluate whether there is a significant difference between the regression slopes m for V_{d}, V_{e}, and V_{n} based on DTMs and DSMs. Table 1 shows that the slopes for the three variables are different, but none of these differences is significant at the 99% confidence level ($p > 0.01$). Only the slopes for V_d are different at the 95% confidence level ($p < 0.05$). In conclusion, it can be stated that the presence of canopy height in the DSMs does not have a major influence on the multi-year volume computations. Most likely, the true elevation changes completely outweigh the vegetation-induced bias, both in magnitude (between −9 and +10 m in 2023) and in spatial extent (Figure 2b). Furthermore, the highest vegetation (sea buckthorn and wild privet) is located mostly outside the polygon used in the volume computations; compare Figure 5a to Figure 2b.

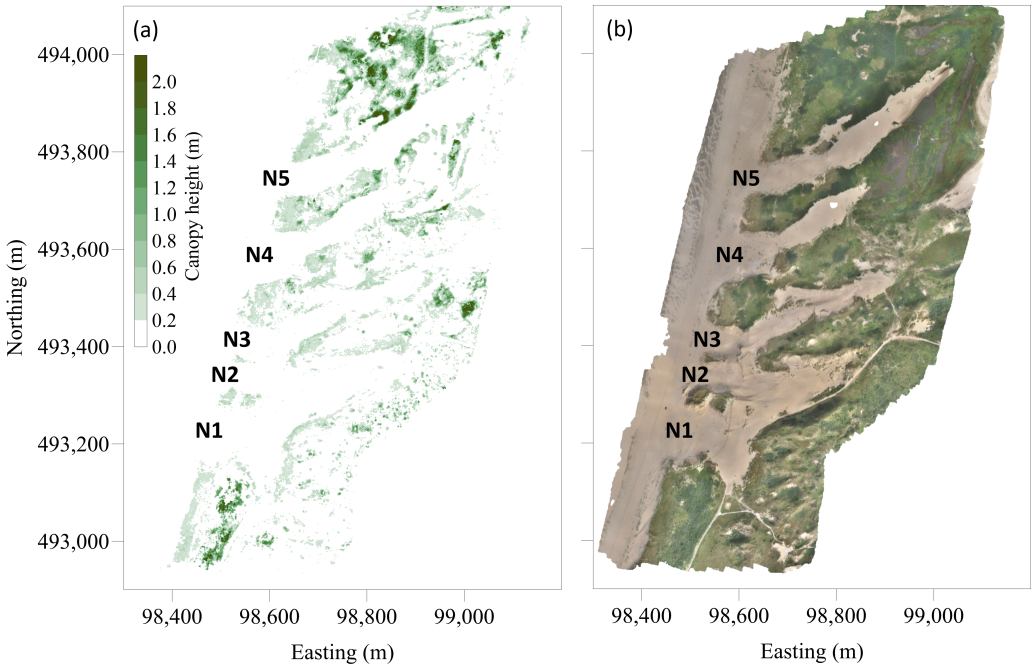

Figure 5. (**a**) DEM of Difference for 2023-02-08 (ALS)–2023-02-13 (UAVSfM) and (**b**) orthomosaic of the 2023-09-25 survey. As explained in the text, the positive elevation differences in (**a**) can here be interpreted as the height of the canopy.

Table 1. Analysis of covariance (ANOCOVA) for linear regression slopes.

	m ALS and UAVLidar m^3/yr	*m* UAVSfM m^3/yr	*F* Statistic	*p* Value
V_d	30,369	33,585	6.87	0.0142
V_e	−15,950	−16,882	0.70	0.4104
V_n	14,420	16,703	2.39	0.1336

Although the previous paragraphs considered vegetation-induced bias in DSMs as a potential limiting factor for their use, a canopy height map, as presented in Figure 5a, is also an important derivative of the current data set and provides opportunities for new research. A map with similar spatial extent and resolution will be virtually impossible to make on the basis of vegetation ground surveys. Potentially, a canopy height map can be used to train and test a machine learning algorithm, such as that presented in [47], to predict and remove vegetation-induced bias in a DSM, in other words, to correct it to a DTM. Another use may be to aid in the prediction of habitat maps from orthomosaics using deep learning. The author of [29] used a Convolutional Neural Network (CNN) with U-net architecture to predict a habitat map from the orthomosaic of 22 March 2022 (with 75% accuracy), with training and testing data derived from vegetation surveys in the field and subsequent visual interpretation of the orthomosaic. Other studies [48,49] have shown that including elevation in the machine learning algorithm can improve the accuracy of prediction. The author of [29] did not obtain any improvement by including elevation, possibly because the habitats in the study region are not limited to unique elevation ranges. Instead, she suggested including cross-shore distance due to the zonation of coastal dune habitats with the distance to the beach [2,50–52]. Figure 5a suggests that including the height of the canopy in the machine learning algorithm can also improve the accuracy of habitat predictions, as habitats have different canopy heights.

Finally, we note that monitoring of the foredune notches and their associated depositional lobes in the NWNKern region will continue in the years to come. We are particularly interested in (i) seeing how long the notches remain corridors for the inland transport of windblown sand and how this depends on the characteristics of the notches, (ii) quantifying

spatio-temporal changes in habitats, and (iii) understanding when and under what environmental conditions vegetation will eventually colonise the notches and depositional lobes, as expected from the biogeomorphic succession of natural notches (trough blowouts, [53,54]). We intend to include newly acquired data in the Zenodo repository by DOI versioning on an annual basis. The DOI provided here (https://doi.org/10.5281/zenodo.7010095, accessed on 11 January 2024) will always resolve to the latest version.

Author Contributions: Conceptualization, G.R., D.G. and B.A.; methodology, G.R.; software, G.R.; investigation, G.R. and B.A.; data curation, G.R.; writing—original draft preparation, G.R.; writing—review and editing, G.R., D.G. and B.A.; funding acquisition, G.R. All authors have read and agreed to the published version of the manuscript.

Funding: The Noordwest Natuurkern project is part of the Dutch Dune Revival project, financed by the European LIFE+ Regulation and the province of North-Holland (LIFE09 NAT/NL/000418). UAV surveys until 2019 were financed by the project "Aeolus meets Poseidon: Windblown Sand Transport on Wave-dominated Beaches" (with project number 13709) of the Vici Research Programme, which is financed by the Dutch Research Council (NWO). Subsequently, the UAV surveys were funded by the Department of Physical Geography and the Earth Simulation Laboratory at Utrecht University.

Institutional Review Board Statement: Not applicable

Informed Consent Statement: Not applicable

Data Availability Statement: The data presented in this study are openly available in https://doi.org/10.5281/zenodo.7010095, accessed on 11 January 2024.

Acknowledgments: We are extremely grateful to all who contributed to the survey data collection, especially Utrecht University technicians and drone experts Henk Markies, Maarten Zwarts, and Marcel van Maarseveen, PWN senior advisor Nature and Recreation Marieke Kuipers, and PWN forest rangers Coen van Oosterom and Imreël van der Sloot. We thank Niels van Kuik (Rijkswaterstaat) for providing additional ALS data (with the help of Ingrid Alkemade) and for expanding the ALS survey region from 2023. Finally, we acknowledge Jelle Treep from Research Data Management Support at Utrecht University for setting up the Agisoft Metashape catalog item in the HPC SURF Research Cloud. Credits for aerial UAV image processing were provided by SURF (project EINF-4926).

Conflicts of Interest: Author Dick Groenendijk was employed by the PWN Drinking Water Company. The remaining authors declare that the research was conducted in the absence of any commercial or financial relationships that could be construed as a potential conflict of interest.

References

1. Balke, T.; Herman, P.M.J.; Bouma, T.J. Critical transitions in disturbance-driven ecosystems: identifying Windows of Opportunity for recovery. *J. Ecol.* **2014**, *102*, 700–708. [CrossRef]
2. Maun, M.A. *The Biology of Coastal Sand Dunes*; Oxford University Press: Oxford, UK, 2009; p. 265.
3. Corenblit, D.; Baas, A.; Balke, T.; Bouma, T.; Fromard, F.; Garófano-Gómez, V.; González, E.; Gurnell, A.M.; Hortobágyi, B.; Julien, F.; et al. Engineer pioneer plants respond to and affect geomorphic constraints similarly along water-terrestrial interfaces world-wide. *Glob. Ecol. Biogeogr.* **2015**, *24*, 1363–1376. [CrossRef]
4. Everard, M.; Jones, L.; Watts, B. Have we neglected the societal importance of sand dunes? An ecosystem services perspective. *Aquat. Conserv. Mar. Freshw. Ecosyst.* **2010**, *20*, 476–487. [CrossRef]
5. Barbier, E.B.; Hackers, S.D.; Kennedy, C.; Koch, E.W.; Stier, A.C.; Silliman, B.R. The value of estuarine and coastal ecosystem services. *Ecol. Monogr.* **2011**, *81*, 169–183. [CrossRef]
6. Nordstrom, K.F.; Arens, S.M. The role of human actions in evolution and management of foredunes in The Netherlands and New Jersey, USA. *J. Coast. Conserv.* **1998**, *4*, 169–180. [CrossRef]
7. Defeo, O.; McLachlan, A.; Schoeman, D.S.; Schlacher, T.A.; Dugan, J.; Jones, A.; Lastra, M.; Scapini, F. Threats to sandy beach ecosystems: A review. *Estuar. Coast. Shelf Sci.* **2009**, *81*, 1–12. [CrossRef]
8. Gao, J.; Kennedy, D.M.; Konlechner, T.M. Coastal dune mobility over the past century: A global review. *Prog. Phys. Geogr.* **2020**, *44*, 814–836. [CrossRef]
9. Nordstrom, K.F.; Jackson, N.L. *Beach and Dune Restoration*, 2nd ed.; Cambridge University Press: Cambridge, UK, 2021; p. 300.
10. Konlechner, T.M.; Ryu, W.; Hilton, M.J.; Sherman, D.J. Evolution of foredune texture following dynamic restoration, Doughboy Bay, Stewart Island, New Zealand. *Aeolian Res.* **2015**, *19*, 208–214. [CrossRef]
11. Darke, I.B.; Walker, I.J.; Hesp, P.A. Beach-dune sediment budgets and dune morphodynamics following coastal dune restoration, Wickaninnish Dunes, Canada. *Earth Surf. Process. Landf.* **2016**, *41*, 1370–1385. [CrossRef]

12. Ruessink, B.G.; Arens, S.M.; Kuipers, M.; Donker, J.J.A. Coastal dune dynamics in response to excavated foredune notches. *Aeolian Res.* **2018**, *31*, 3–17. [CrossRef]
13. Hilgendorf, Z.; Walker, I.J.; Pickart, A.J.; Turner, C.M. Dynamic restoration and the impact of native versus invasive vegetation on coastal foredune morphodynamics, Lanphere Dunes, California, USA. *Earth Surf. Process. Landf.* **2022**, *47*, 3083–3099. [CrossRef]
14. Nguyen, D.; Hilton, M.; Wakes, S. Aeolian sand transport thresholds in excavated foredune notches. *Earth Surf. Process. Landf.* **2022**, *47*, 553–568. [CrossRef]
15. Walker, I.J.; Hilgendorf, Z.; Gillies, J.A.; Turner, C.M.; Furtak-Cole, E.; Nikolich, G. Assessing performance of a "nature-based" foredune restoration project, Oceano Dunes, California, USA. *Earth Surf. Process. Landf.* **2023**, *48*, 143–162. [CrossRef]
16. Lithgow, D.; Martínez, M.L.; Gallego-Fernández, J.B.; Hesp, P.A.; Flores, P.; Gachuz, S.; Rodríguez-Revelo, N.; Jiménez-Orocio, O.; Mendoza-González, G.; Álvarez-Molina, L.L. Linking restoration ecology with coastal dune restoration. *Geomorphology* **2013**, *199*, 214–224. [CrossRef]
17. Martinez, M.L.; Gallego-Fernandez, J.B.; Hesp, P.A. *Restoration of Coastal Dunes*; Springer Verlag: Berlin, Germany, 2013; p. 347.
18. Emery, S.M.; Rudgers, J.A. Ecological assessment of dune restorations in the Great Lakes Region. *Restor. Ecol.* **2010**, *18*, 184–194. [CrossRef]
19. Derijckere, J.; Strypsteen, G.; Rauwoens, P. Early-stage development of an artificial dune with varying plant density and distribution. *Geomorphology* **2023**, *437*, 108806. [CrossRef]
20. Johnston, K.K.; Dugan, J.E.; Hubbard, D.M.; Emerry, K.A.; Grubbs, W.M. Using dune restoration on an urban beach as a coastal resilience approach. *Front. Mar. Sci.* **2023**, *10*, 1187488. [CrossRef]
21. Arens, S.M.; Mulder, J.P.M.; Slings, Q.L.; Geelen, L.H.W.T.; Damsma, P. Dynamic dune management, integrating objectives of nature development and coastal safety: Examples from the Netherlands. *Geomorphology* **2013**, *199*, 205–213. [CrossRef]
22. Gann, G.D.; McDonald, T.; Walder, B.; Aronson, J.; Nelson, C.R.; Jonson, J.; Hallett, J.G.; Eisenberg, C.; Guariguata, M.R.; Liu, J.; et al. International principles and standards for the practice of ecological restoration. Second edition. *Restor. Ecol.* **2019**, *27*, S1–S46. [CrossRef]
23. IUCN. *Guidance for Using the IUCN Global Standard for Nature-Based Solutions. A User-Friendly Framework for the Verification, Design and Scaling up of Nature-Based Solutions*, 1st ed.; Technical Report; IUCN: Gland, Switzerland, 2020. [CrossRef]
24. Pickart, A.J. Ammophila invasion ecology and dune restoration on the West Coast of North America. *Diversity* **2021**, *13*, 629. [CrossRef]
25. Kuipers, M. The daring Dutch: Restoring the dynamic dunes. In Proceedings of the Coastal Dunes Management Strategies and Practices: Perspectives and Case Studies, Pas-de-Calais, France, 17–19 June 2014; Favennac, J.; Battiau-Queney, Y., Eds.; Dynamiques Environnementales: Pesac, France, 2014; Volume 33, pp. 132–138.
26. Van Hateren, J.A.; Van Buuren, U.; Arens, S.M.; Van Balen, R.T.; Prins, M.A. Identifying sediment transport mechanisms from grain size-shape distributions, applied to aeolian sediments. *Earth Surf. Dyn.* **2020**, *8*, 527–553. [CrossRef]
27. Kooijman, A.M. *Environmental Problems and Restoration Measures in Coastal Dunes in The Netherlands*; Springer: Berlin/Heidelberg, Germany, 2004; Chapter 15, pp. 243–258.
28. Ruessink, G.; Arens, B.; Kuipers, M. Multi-annual geomorphic evolution of excavated foredune notches. In Proceedings of the EGU General Assembly 2022, Vienna, Austria, 23–27 May 2022. [CrossRef]
29. Kooij, F. Classification of Coastal Dune Vegetation from Aerial Imagery with a Convolutional Neural Network. Master's Thesis, Utrecht University, Utrecht, The Netherlands, 2022.
30. Ouwerkerk, T. Habitat Mapping from High-Resolution UAV Orthomosaics Using Convolutional Neural Networks. Master's Thesis, Utrecht University, Utrecht, The Netherlands, 2023.
31. Urson, M. Comparing Seasonally-Varied CNNs in Vegetation Segmentation Performance. Master's Thesis, Utrecht University, Utrecht, The Netherlands, 2023.
32. Luijendijk, A.; De Vroeg, H.; Swinkels, C.; Walstra, D.J. Coastal response on multiple scales: A pilot study on the IJmuiden port. In Proceedings of the Coastal Sediments, Miami, FL, USA, 2–6 May 2011; pp. 602–615.
33. Hallin, C.; Huisman, B.J.A.; Larson, M.; Walstra, D.J.R.; Hanson, H. Impact of sediment supply on decadal-scale dune evolution—Analysis and modelling of the Kennemer dunes in the Netherlands. *Geomorphology* **2019**, *337*, 94–110. [CrossRef]
34. Kuipers, M.; Arens, B.; Ruessink, G. Grootschalig herstel van stuivende duinen. *Levende Nat.* **2016**, *117*, 89–93. (In Dutch)
35. Groenendijk, J. *088 Kennemerland-Zuid PAS-Gebiedsanalyse: Update AERIUS Monitor 2016L. Rapport WATE_BE4725_R001F01*; Technical Report; HasKoningDHV Nederland B.V.: Amsterdam, The Netherlands, 2017. (In Dutch)
36. Arens, S.M.; Geelen, L.H.W.T. Dune landscape rejuvenation by intended destabilisation in the Amsterdam Water Supply Dunes. *J. Coast. Res.* **2006**, *225*, 1094–1107. [CrossRef]
37. Taddia, Y.; Stecchi, F.; Pellegrinelli, A. Coastal Mapping Using DJI Phantom 4 RTK in Post-Processing Kinematic Mode. *Drones* **2020**, *4*, 9. [CrossRef]
38. Nota, E.W.; Nijland, W.; de Haas, T. Improving UAV-SfM time-series accuracy by co-alignment and contributions of ground control or RTK positioning. *Int. J. Appl. Earth Obs. Geoinf.* **2022**, *109*, 102772. [CrossRef]
39. Over, J.R.; Ritchie, A.C.; Kranenburg, C.J.; Brown, J.A.; Buscombe, D.; Noble, T.; Sherwood, C.R.; Warrick, J.A.; Wernette, P.A. *Processing Coastal Imagery with Agisoft Metashape Professional Edition, Version 1.6—Structure from Motion Workflow Documentation: U.S. Geological Survey Open File Report 2021-1039*; Technical Report; U.S. Geological Survey: Reston, VA, USA, 2021. [CrossRef]
40. The MathWorks Inc. *Matlab Version: 9.14.0.2337262 (R2023a) Update 5*; The MathWorks Inc.: Natick, MA, USA, 2023.

41. Schwanghart, W.; Scherler, D. TopoToolbox 2—MATLAB-based software for topographic analysis and modeling in Earth surface sciences. *Earth Surf. Dyn.* **2014**, *2*, 1–7. [CrossRef]
42. Bochev-van der Burgh, L.M.; Wijnberg, K.M.; Hulscher, S.J.M.H. Decadal-scale morphologic variability of managed coastal dunes. *Coast. Eng.* **2011**, *58*, 927–936. [CrossRef]
43. De Vries, S.; Southgate, H.N.; Kanning, W.; Ranasinghe, R. Dune behavior and aeolian transport on decadal timescales. *Coast. Eng.* **2012**, *67*, 41–53. [CrossRef]
44. Ruessink, G.; Schwarz, C.S.; Price, T.D.; Donker, J.J.A. A multi-year data set of beach-foredune topography and environmental forcing conditions at Egmond aan Zee, The Netherlands. *Data* **2019**, *4*, 73. [CrossRef]
45. Anders, N.; Valente, J.; Masselink, R.; Keesstra, S. Comparing filtering techniques for removing vegetation from UAV-based photogrammetric point clouds. *Drones* **2019**, *3*, 61. [CrossRef]
46. Rotnicka, J.; Dluzewski, M.; Dabski, M.; Rodzewicz, M.; Slodarski, W.; Zmarz, A. Accuracy of the UAV-based DEM of beach-foredune topography in relation to selected morphometric variables, land cover, and multitemporal sediment budget. *Estuaries Coasts* **2020**, *43*, 1939–1955. [CrossRef]
47. Enwright, N.M.; Kranenburg, C.J.; Patton, B.A.; Dalyander, P.S.; Bronw, J.A.; Piazza, S.C.; Cheney, W.C. Developing bare-earth digital elevetion models from structure-from-motion data on barrier islands. *ISPRS J. Photogramm. Remote Sens.* **2021**, *180*, 269–282. [CrossRef]
48. Kattenborn, T.; Eichel, J.; Fassnacht, F.E. Convolutional Neural Networks enable efficient, accurate and fine-grained segmentation of plant species and communities from high-resolution UAV imagery. *Sci. Rep.* **2019**, *9*, 17656. [CrossRef]
49. Cruz, C.; O'Connell, J.; McGuinness, K.; Martin, J.R.; Perrin, P.M.; Connolly, J. Assessing the effectiveness of UAV data for accurate coastal dune habitat mapping. *Eur. J. Remote Sens.* **2023**, *56*, 219870. [CrossRef]
50. Bakker, J.P. Phytogeographical aspects of the vegetation of the outer dunes in the Atlantic province of Europe. *J. Biogeogr.* **1976**, *3*, 85–104. [CrossRef]
51. Doing, H. Landscape ecology of the Dutch coast. *J. Coast. Conserv.* **1995**, *1*, 145–172. [CrossRef]
52. Lalimi, F.Y.; Silvestri, S.; Moore, L.J.; Marani, M. Coupled topographic and vegetation patterns in coastal dunes: Remote sensing observations and ecomorphodynamic implications. *J. Geophys. Res. Biogeosci.* **2017**, *122*, 119–130. [CrossRef]
53. Schwarz, C.; Brinkkemper, J.; Ruessink, G. Feedbacks between biotic and abiotic processes governing the development of foredune blowouts: A review. *J. Mar. Sci. Eng.* **2019**, *7*, 2. [CrossRef]
54. Van Kuik, N.; De Vries, J.; Schwarz, C.; Ruessink, G. Surface-area development of foredune trough blowouts and associated parabolic dunes quantified from time series of satellite imagery. *Aeolian Res.* **2022**, *57*, 100812. [CrossRef]